Jurnal Tribologi 24 (2020) 80-99

Jurnal Tribologi
Website : jurnaltribologi.mytribos.org
e-issn: 2289-7232

The morphological and surface roughness of magnetorheological polished AISI 6010 surface

Soffarina M. Soffie [1], Izwan Ismail [1*], Mutalib A. Nurain [1], Syarifah N. Aqida [2]

[1] Faculty of Manufacturing and Mechatronic Engineering Technology, College of Engineering Technology, Universiti Malaysia Pahang, 26600 Pekan, Pahang, MALAYSIA.
[2] Faculty of Mechanical Engineering, College of Engineering, Universiti Malaysia Pahang, 26600 Pekan, Pahang, MALAYSIA.
[*]Corresponding author: izwanismail@ump.edu.my

KEYWORDS

AISI 6010 Aluminium Surface
Magnetorheological polishing
Surface Roughness Reduction Ratio

ABSTRACT

This paper discussed the morphological and surface roughness produced on AISI 6010 aluminium surface with microgroove using the magnetorheological polishing method. Initially, the 17 samples were prepared with micro v-groove features using CNC (computer numerical control) milling machine. Box-Behnken design of experiment (DOE) was used to vary the polishing process factors namely; speed, voltage, and magnetic field. The DOE allows a relationship on morphological and surface roughness to be studied. The MRP process is carried out using fabricated 1 axis 2 d.o.f MRP rig mounted on a CNC machine. Abrasive added MRP fluid was used during the polishing process. The surface roughness, Ra, of the samples was measured under an Olympus 3D laser microscope. From morphology study, the irregularities on v-groove and the flat surface of 17 samples after MRP were reduced. The magnetorheological polishing process reduced surface roughness from 10 μm to as low as 0.4 μm with a constant polishing time of 10 minutes. This study shows that the MRP method is capable to replace the conventional polishing process to polish complex micro features on Al 6010 surface.

Received 21 October 2019; received in revised form 8 January 2020; accepted 13 February 2020.
To cite this article: Soffie et al. (2020). The morphological and surface roughness of magnetorheological polished AISI 6010 surface. Jurnal Tribologi 24, pp.80-99.

1.0 INTRODUCTION

Recent technological advancement in the field of polishing finishing led to increasing demand for micro mould technology that grew rapidly over the years. Micro-mould surface requires to produce a smoother and superior surface. This extreme precision is to enhance and enable micro-mould product to perform exceptionally. Several machines and techniques were proposed such as variation of parameter, magnetic field, and type of material samples. The micro-milling approach is preferable for the metal micro-mould product as it a simple setup, low cost, and flexibility of design. Nonetheless, exploring details on techniques of MR polishing finishing is necessary to reinforce the performance.

MR fluids have been viewed as one of the smart material due to its capability to change rheological properties by altering magnetic field supply (Kang et al.,2009), (Wiltsie et al., 2012). In the absence of a magnetic field, MR fluid behaves like Newtonian fluid (Kang et al.,2009) with constant viscosity. In the presence of the magnetic field, MR fluid behaviour turns into Bingham plastic; a yield-stress fluid that is able to maintain stress within the particles that are unable to flow (Wiltsie et al. 2012). The smart fluid consists of a ratio of magnetically polarize particles such as carbonyl-iron particles (CIP), alumina and a carrier liquid such as silicone oil, synthetic oil, water, and mineral oil. The particles of MR fluid is well known with soft magnetic materials and able to control its rheological properties. Carbonyl iron particle (CIP) is widely used due to its higher magnetic permeability (Kang et al.,2009). The magnetic particles were aligned in a chain structure on its dipole along the field direction and the thermal energy increased when the energy was applied to the particles by a magnet and the non-magnetic particles align proportionally with the magnetic field strength (Rahim et al., 2016). These fluids are vastly known in applications such as dampers, torque, robotic, vibration control system, transducers and are a great potential for the automotive industry (Kang et al. 2009; Skalski & Kalita 2017).

Metal surfaces are produced by a variety of material removal processes which practically subjected to wear and friction. The surface profiles are varies depending on the machine and tooling. The metal surface can be associated with a deformation process in both tools and workpieces. Friction induced temperature generation and multicyclic motion during machining process affecting the finishing accuracy (Abukhshim et al., 2006). This behaviour might due to tool wear that directly affecting the surface roughness. Lowering the surface roughness is the prime objective in many research (Senthil Kumar et al. 2013; Wang et al. 2016; Song et al., 2013; Tingzhang et al., 2015). Surface roughness is a resultant of many factors, including cutting parameters, tool geometry, workpiece material, and lubricant. In the case of microchannel on microfluidic devices, surface roughness of the channel determines the flow characteristic for a specific application, therefore producing finished surface at precise roughness is a requirement.

Another cause of surface roughness is burr formation in micro-milling. Three types of burrs that aroused in micro-milling which are top burr, exit burr, and entrance burr. The top burr is located on the top surface of the workpiece while the exit burr is located at the exit position of a cutting tool (Saptaji & Subbiah 2017). The entrance burr is located at the entrance position of the cutting tool and able to push the material to formed top burr. As the high precision manufacturing become a requirement to produce precision parts in mechanical-electronic devices, micro-milling of a micro mould become essential. Therefore, the burr produced with micro-milling has to be removed through ultra-precision polishing. Ultraprecision polishing used in processing various materials including micro bulk silicon and aluminium. The problem of polishing micro features is to obtain desired roughness without disrupting the micro mould precision. The micro features are easily damaged during conventional deburring procedures and it is difficult to remove burr

(Jang et al., 2012). The burr formation may disrupt performance efficiency; therefore, it requires high attention to handling the micro mould product during polishing.

1.1 Magnetorheological Polishing

Conventional or traditional polishing is a process that requires physical, time consumption and skills to obtain precise finishing (Liu et al., 2016)(Tricard et al., 2003). Complex geometry on micro mould consists of a small interior that is not capable to polish with conventional polishing. One of the conventional polishing methods is wet etching machining that provides a high material removal, only applicable to isotropic etching and is not suitable for the high-precision shape and dimensional control. The solution is to use dry etching but on the other hand, dry etching often has a low etching rate and thus a high machining cost (Kolari 2008) (Park et al., 2005). Another method of conventional polishing is the lapping process. Lapping is one of the processes that contain abrasive granules which cover a small fraction, at low abrasive concentrations. The abrasives are capable of sticking on the additional space of a surface due to the increment of surface density (Evans et al., 2003). The drawback of lapping is the surface density during constant speed because there is no space for an additional abrasive during high abrasive concentration (Evans et al., 2003).

A better solution is by using MR polishing that has the capability to polish surface on complex geometry and on a micro mould scale size. Surface roughness and burrs can be removed on both flat and groove surfaces. This process is suitable for both ferromagnetic and non-magnetic material such as aluminium, copper, glass (Cheng et al., 2009), fused silica and mild steel (Kumar Singh et al., 2012). This method has been used to polish curved mirror surfaces and other glasses material (Gopal et al., 2017) (Lambropoulos et al. 2010). There are few studies conducted on the polishing of metal surfaces. Most of the researcher has developed variety of MR polishing machine method that polish on different types of glasses, silicon, crystal, and optical ceramics (Tricard et al., 2003)(Luo et al., 2005)(Cheng, Feng, et al. 2009)(Sidpara & Jain 2012)(Liu et al. 2016)(Wang et al., 2016)(Gopal et al., 2017)(Cheng, Yam et al., 2009)(Lambropoulos et al. 2010)(Kim et al., 2008)(Miao et al., 2009). An automated five-axis CNC ball end that polish freeform mild steel workpiece has been designed by the Indian Institute of Technology, Delhi, in 2018 (Alam et al., 2018).

In addition, (Wang et al., 2015) investigated the optical surface where magnetorheological polishing fabrication employed a rheological modification of MR fluid with the magnetic field gradient to create a flexible and highly stable 'sub-aperture polishing lap'. There are three basic orientations between the magnetic field and shear direction which depends on yield stress where the increasing volume fraction of magnetic particles increases the dynamic yield stress of MR fluid (Saraswathamma et al., 2015). This is because finer particles tend to have vary thermal and have a lower magnetisation where magnetic suspension yield stress of the fluid is proportional to the square of magnetisation (Saraswathamma et al., 2015).

Surface finish and production rate is important with increasing demands of precision finished products in various markets (Kumar Singh et al. 2012). It created a smooth, damage-free surface finish rather than conventional polishing where the particle's normal load result in scratching (Tricard et al., 2003). Using this type of polishing subsurface damage and residual stress can be removed therefore, the surface roughness decreased.

1.2 Material Removal Mechanism In Magnetorheological Polishing

There are different ways of polishing surface roughness or asperities. One of the findings is MR fluid filled the gap of the asperities and Cheng verified that material removal occurred through shear stress created that being dragged into the gap (Cheng et al., 2009). Material removal increased due to higher strength of magnetic field and therefore, higher viscosity generated higher shear forces in the polishing processes. Increased mixing ratio of abrasive particles in the fluid therefore, more abrasives would be engaged in polishing within a unit time (Cheng, Yam, et al., 2009) to obtained higher material removal rates. The material removal rate and surface roughness of polishing were measured by altering electric currents, feed, and speed of CNC (Kim et al., 2008). Kim observed that after a certain speed, the rate removed depth decelerates due to excessive yield stress which destroys the chain structures among the particles (Kim et al., 2008). Moreover, it can lead to slipping of the particles between the wheel surface and MR fluid.

The purpose of this research is to reduce surface roughness on AISI 6010 aluminium by magnetorheological ultra-precision polishing. In this work, a smaller size abrasive of 500 nm was used to investigate the effect of material removal rate and surface roughness reduction ratio on the process parameters. Altering the process parameter (magnetic field, polishing gap, and rotational speed) on MR polishing rig was able to reduce the surface roughness of finishing surfaces. Morphological and surface roughness produced on AISI 6010 aluminium surface using the MRP method was discussed.

2.0 EXPERIMENTAL SETUP

Magnetorheological polishing rig setup is as shown in the schematic diagram of Figure 1. The machine was made with a different type of ferromagnetic and nonmagnetic material. Magnetic field distribution of the machine was identified through finite element simulation using a finite element method for magnetic (FEMM) software before fabrication. The stationary electromagnet coil was wired on the rig to distribute magnetic flux density. The MR machine was fixed on the CNC vice on the x-y-z axis movement table. The MR fluid filled in the base plate to polish the workpiece. With the presence of the magnetic field, the MR fluid solidified in milliseconds and dispersed. The special characteristic of abrasive is the sharp polygonal shapes that enhance MR fluid to polish complex micro mould geometry. The MR holder was placed in the chuck on a fixed X-Y axis. The holder consists of four slots to hold the workpiece which a mass production undergoes polishing is capable to save time massively. The copper wire of the electromagnetic coil was connected to a relay and Quantel QPS-HD D.C power supply as shown in Figure 3 Quantel QPS-HD D.C power supply is used to control the magnetic current on electromagnet coil. The variation of electromagnet of MR was monitored using gauss meter.

The carbonyl iron particles (CIP) were aligned along the magnetic flux direction which aided the abrasive particle towards the end of MR fluid tip. Figure 2(a) shows an example of a demonstration of scattered MR fluid on the base plate during the presence of the magnetic field. The amount of material abraded from the surface roughness peaks of the workpiece surface by abrasives depends on the voltage applied to the power supply. The abrasives majority were moved away from the electromagnetic coiled wire due to the magnetic forces that pushed the abrasive towards the surface of the workpiece. MR fluid behaves as a non-Newtonian fluid without the presence of the magnetic field. The higher the yield stress of MR fluid, the stronger the bond of CIP chains surrounding the abrasive particles which firmly hold for a long time under

high shear strength to abrade the surface with an efficient material removal rate (Kumar Singh et al. 2012).

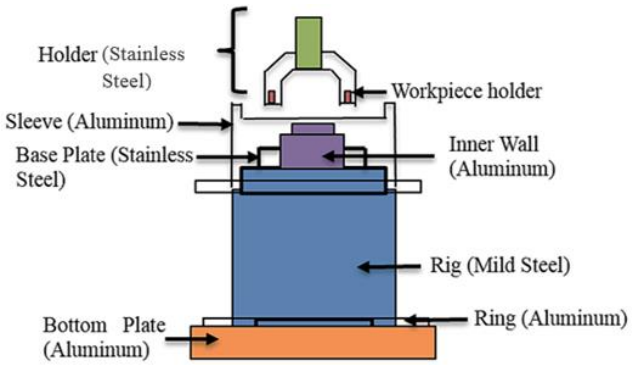

Figure 1: Schematic polishing mechanism of magnetorheological polishing setup.

Figure 2: MR fluid (a) with the presence of a magnetic field and (b) without the presence of magnetic field.

The fabricated MR polishing rig was analysed using a finite element method for magnet (FEMM), the experiments were performed on a v-groove aluminium AISI 6061 using 1 axis 2 d.o.f MRP rig which is mounted on a CNC machine as shown in Figure 3. The MR machine was coiled with copper wire with a diameter of 0.65mm and 2040 turn around the core to supply the magnetic field. The amount of magnetic flux density was altered by Quantel QPS-HD power supply create a chain-like formation process in MR fluid that solidifies the liquid. The most important part of the machine is the electromagnet that activates and distribute magnet. The machine was tested using a gaussmeter to analyse the present magnetic field and adjusting magnetic poles. The workpiece v-grooves were prepared by a high-speed milling process on CNC vertical milling machine with a rotational speed of 2443 m/s. The initial range of surface roughness, R_a obtained was 0.3 - 8.7 µm after high-speed milling.

The sample used in the simulation was the magnetorheological fluid, MRF-132DG, a commercial MR fluid. The minimum magnetic flux density required to develop chain formation for MRF-132DG is approximately 0.0597 T (Wiltsie et al., 2012). As the MRF-132DG has a minimum of 0.0587 T, therefore in the experiment, the fluid changed into MR fluid that consists of the composition shown in Table 3 that has 0.62824 T minimum magnetic flux density at a current of 3 A.

2.1 Design of Experiment

The Box-Behnken design was used to develop samples with three factors of rotating speed, polishing gap, and voltage. The application of RSM on polishing of AISI 6061 aluminium was carried out to develop a mathematical model for surface roughness R_a Table 1 shows 17 experiment parameters resulted from the Box -Behnken design. The MR fluids were optimised for maximum material removal rate and surface roughness reduction ratio.

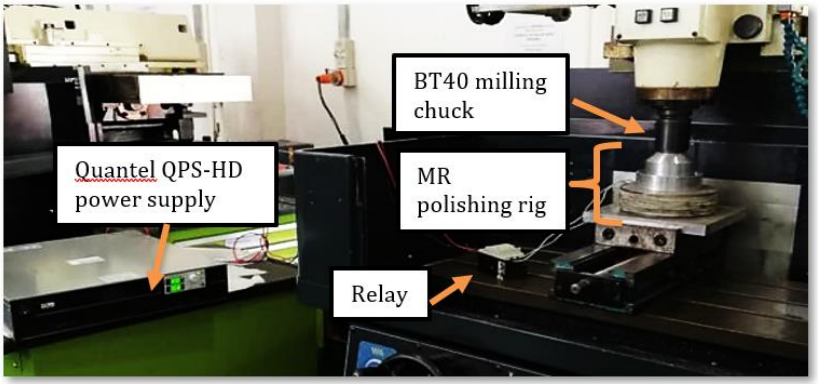

Figure 3: Magnetorheological polishing rig setup.

Table 1: Corresponding actual values of process parameter.

Sample no.	MR processing parameters			Output parameters	
	Voltage (V) (X_1)	**Rotational Speed (m/s) (X_2)**	**Polishing Gap (mm) (X_3)**	**MRR (mm/sec)**	**SRRR (**mm^3/ sec **)**
1	75	500	3	7.088	15.168
2	120	50	2	23.665	9.819
3	75	50	3	16.277	8.632
4	75	252.5	2	20.036	15.814
5	75	252.5	2	13.025	10.286
6	30	252.5	1	6.312	2.7378
7	30	500	2	10.432	14.748
8	30	50	2	3.076	5.0833
9	120	252.5	3	7.529	7.371
10	30	252.5	3	6.097	19.106
11	75	252.5	2	14.394	14.067
12	75	252.5	2	19.506	9.168
13	120	252.5	1	18.659	12.279
14	120	500	2	18.437	18.247
15	75	252.5	2	19.302	9.067
16	75	50	1	18.089	7.669
17	75	500	1	9.688	8.981

Table 2: Experimental parameter on MR polishing.

Workpieces dimension	Aluminium AISI 6061 V –groove (d=1mm, w= 3mm, α= 90°)
Polishing tools	1 axis 2 d.o.f MRP rig mounted on CNC machine
Polishing fluid	Water based (deionized water)
Abrasives	Alumina (sharp polygonal shapes with grain size 500nm)
MR fluid cycle	2 cycles
Polishing time, t	10 min
Rotational speed,	50-500 m/s
Voltage	30-120 V
Polishing gap (mm)	1-3 mm

During the experiment, MR fluid composition, polishing cycle, polishing time, workpiece dimension, fluid height was selected as control factors as shown in Table 2. The MR fluid cycles were constant where the usage of MR fluid used for two-cycle per workpiece. The polishing time was set to 10 minutes as the machine able to withstand heat temperature 45.82T with 120V. The MR abrasive and MR composition were kept constant as, before the polishing process, another variety sets of samples were analysed. The sets of samples were analysed using MRR significant parameters of 1mm, 120V, and 50m/s. The workpiece was attached with a permanent magnet near the v-groove before inserting it into one of the four slots. This preparation is important to obtain a higher magnetic flux density adjacent to the desired polishing area for better performance on surface roughness.

The top of the base plate was set as the origin that can be centred to the position of the desired polishing gap. The holder was set on x-, y- and z-axis relative to the reference of the inner wall. The x- and y-axis setting is more important compared to the z-axis because the holder may hit the inner wall during polishing and distorts the top part of holder. The distortion of the top part of the holder may create a non-harmonic rotation (or wobble). MR fluid was added into the base plate at a constant height of 2 mm to rotate the holder at 2 d.o.f on a CNC vice. A workpiece of a 24×26 mm dimension with v-groove was attached in one of the four slots and polished in the x-y direction. The full setup is as shown in Figure 3.

2.2 Magnetorheological Fluid

The MR fluid components are carbonyl iron particle (CIP), glycerol, $H_2\,O$, $Al_2\,O_3$ particles with deionised water as the carrier fluid. The CIP with 3-5 μm of average particle size was used as the magnetic media to aid the abrasive alumina as a polishing agent with a size of 500 nm. The sharp polygonal shapes alumina powder fits into small complex geometry, in this case, is v-groove to ease the polishing process. Glycerine was added in the MR fluid to enhance the attachment of other components and act as corrosion resistance. The density and volume percentage of the components in MR fluid is shown in Table 3. Glycerine was mixed with deionised water, DI water in a beaker while weighing the weight of the composition. The solution was stirred for 10 minutes by using an overhead stirrer at 800 rpm. At the same time, an ultrasonic bath (Branson 3800 CPXH Series) was homogenised to 57-60°C for 1 hour. The preparation process of MR fluid is shown in Figure 4. These steps were done to avoid aggregation of particles and to remove air from the solution. The solution was mixed with CIP and stirred for 15 minutes. Finally, abrasive alumina was added and stirred for 15 minutes. The ultrasonic bath was degassed for 30 minutes without

the mixture to remove bubbles formation during agitation while the mixture in the beaker was homogenised for 1 hour. MR fluid was kept into room temperature for one week before the water effected on CIP and became rust after one week.

Table 3: Components in MR fluid.

Component	Density (g/mL@ g/ cm^3)	Vol%
CIP	7.86	40
H20	1.00	50
Glycerol	0.97	5
AL2O3	4.00	5

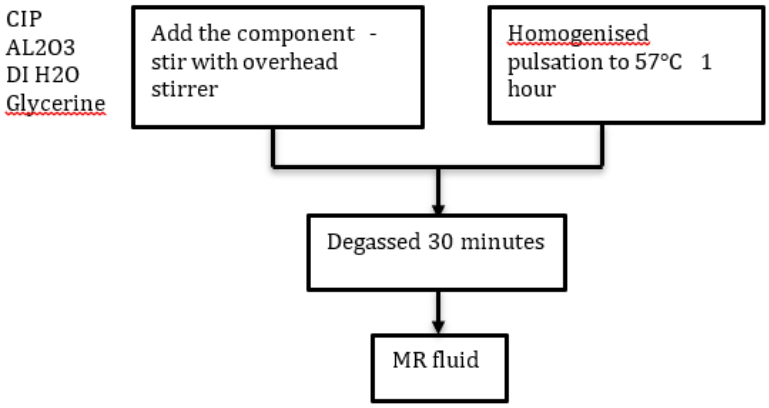

Figure 4: MR fluid preparation steps.

2.3 Workpiece Preparation

The workpiece material used as the test specimen was 150 mm × 450 mm square flat AISI 6061 aluminium alloy bar with a hardness of 40HRB were cut by band saws with 3820 rpm. The workpiece was machined into 26 mm x 24 mm using large-diameter replaceable carbide-insert face milling cutters at speed and feed rate of 1000 rpm and 100 mm/min respectively as shown in Figure 5. The shape of the workpiece was machined with a solid carbide 4 flute square end mill with a diameter of 18 mm. Lastly, a chamfering end mill tool with two flutes (code no: K2EC 090 060C) from Precisetech Sdn. Bhd was used for grooving the v-groove. The v-groove formed at the edge of chamfer with d=1mm, w= 3mm v-groove dimension. The specifications of the tool are presented in Table 4. The CNC machine was set at 2 axis 3 d.o.f with speed and feed rate of 2957 rpm and 140 mm/min respectively.

The samples were characterised for morphology study by video measurement Microscope Profile Video Measurement System (Seven Ocean Optical Technology) and Keyence 3D Laser Scanning Confocal Microscope (VK-X Series, America). Video measurement is to investigate and measure the sample profile. Whereas, the laser microscopy is to measure the groove profile and surface roughness and roughness reduction ratio by using ISO 13565-2 and ISO 13565-3 standard.

Table 4: Tool details.

Tool type	K2EC 090 060C
Tool material	Solid carbide
Number of flutes	2
Diameter	6 mm
Shank	6 mm
Angle	90°
Cutting flute length	14 mm
Total length	57 mm

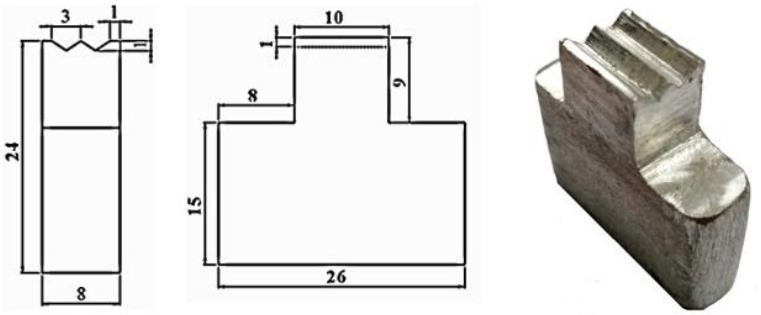

Figure 5 (a) Side; (b) front view of the workpiece; and (c) photograph of the workpiece.

3.0 RESULTS AND DISCUSSION

3.1 Material Removal Rate and Surface Roughness Reduction Ratio

The analysis was carried out using Analysis of Variance, ANOVA as indicated in Table 5. A polynomial equation was generated for voltage, polishing gap, and rotational speed. The parameters were evaluated using F-test and p-value. The ANOVA table for material removal rate, MRR, and surface roughness reduction ratio, SRRR response shows that the quadratic model is statistically significant evidence at α=0.05. The p-value of ANOVA on MRR and SRRR is 0.0270 and 0.0021 respectively indicates the model is significant. Based on ANOVA in MRR model where A, C, AB, C^2 are significant model terms, meanwhile, SRRR model obtained A, B, C, AC as a significant model term. MRR lack of fit value of 4.73 implies chance the model is fitted with 8.37% due to large noise while SRRR the lack of fit value is 0.87 implies 58.12% chance due to noise or vibration. A large lack of fit on the p-value shows that the model is fit. The percentage contribution of the parameter that influences the material removal rate is also presented in Table 5. The lack of fit for better data by changing linear regression to a polynomial regression by adding a quadratic term. The percentage contribution of various polishing parameters such as voltage, speed, gap and the interactions that influence the surface roughness reduction ratio are presented in the same table in Table 5. The highest contribution in this polishing experiment is the voltage as it supplies and activated the magnetic field towards the whole MR polishing machine thus towards the polishing process.

Logarithmic transformations of base 10 were used to express material removal rate (MRR), $Log_{10}MRR$ due to large response ranges from 3.076 to 23.665 which is greater than 10. The ratio

of maximum to a minimum is 7.6934. The ratio of more than 10 required transformations. On the other hand, Surface Roughness Reduction Ratio, SRRR ratios less than 3 the power transforms have a little effect and the response ranges from 2.738 to 19.106. The ratio of maximum to a minimum is 6.9783. SRRR logarithmic transformations were expressed as $Log_{10}SRRR$. For both MRR and SRRR, the independent variables x_1,x_2, x_3 shown in Table 5 were optimally distributed by Box-Behnken for efficient construction of a quadratic model in response surface methodology.

Table 5: ANOVA and regression analysis table for MRR and SRRR analysis.

Source	Mean Square		F value		p-value (Prob > F)				
					ANOVA		Regression		
	MRR	SRRR	MRR	SRRR	MRR	SRRR	MRR	SRRR	
Model	0.093	0.100	4.66	8.22	0.027	0.002			*
A-voltage	0.40	0.067	20.37	5.50	0.003	0.041	0.050	0.006	
B-speed	0.054	0.11	2.71	8.94	0.144	0.014	0.790	0.876	
C-gap	0.16	0.080	8.04	6.54	0.025	0.028	0.967	0.016	
AB	0.14	$1.33 \times 10^{-0.003}$	7.09	0.11	0.032	0.748	0.194	0.594	
AC	0.036	0.28	1.81	23.35	0.220	0.001	0.323	0.002	
BC	0.061	$4.70X10^{-0.003}$	3.06	0.39	0.124	0.548	0.036	0.481	
A^2	$8.49 \times 10^{-0.003}$	-	0.43	-	0.534	-			
B^2	0.052	-	2.63	-	0.149	-			
C^2	0.26	-	13.02	-	0.009	-			
Residual	0.020	0.012							
Lack of Fit	0.036	0.011	4.73	3.99	0.084	0.581	0.082	0.747	●

* Significant ●Not Significant

Table 6: R-Squared, Adjusted R-Squared and Predicted R-Squared.

	MRR	SRRR
R-Squared (%)	85.70	83.15
Adj R-Squared (%)	67.32	73.04
Pred R-squared (%)	-10.25	44.63

From Figure 6, The R-Squared for MRR and SRRR obtained indicates that the model explains all the variability of the response data around its mean. The R-squared is higher which the model fits your data as shown in table 4.2. Theoretically, the model could explain 85.70 % of MRR variance and 83.15 % of SRRR variance, the fitted values are almost equal to the observed values. The adjusted R-squared is a modified version of R-squared that has been adjusted for the number of predictors in the model. The Adjusted R-Squared of MRR and SRRR which are 67.32% and 73.04% respectively improves the model more than would be expected by chance. The predicted R-squared indicates a regression model predicts the responses. A higher-order polynomial due to many predictors begins to model random noise in the data which is known as overfitting the model. The predicted R-squared for both MRR and SRRR is not a significant parameter to evaluate a model.

Mathematically, the quadratic relationship for the studied variables was expressed in the following equation for MRR and SRRR:

$$Log10(MRR) = -0.451 + 0.846X_1 + 1.405E-005X_2 + 0.017\,X_3 + 7.563E-004\,X_1X_2 - 2.106E-003X_1X_3 - 1.561E-003X_2X_3 - 0.267\,X_1{}^2 - 2.450E-006\,X_2{}^2 - 2.424E-005\,X_3{}^2 \quad (1)$$

$$Log10(SRRR) = -0.331 + 0.014X_1 + 2.637E-004X_2 + 0.503\,X_3 - 5.919E-003X_1X_3 - 1.514E-006\,X_1\,X_2 + 1.906E-004\,X_2\,X_3 \quad (2)$$

The optimization plot shows the effect of each factor in columns on the responses or composite desirability in the rows. The vertical red lines and the red number on the graph represent the current factor settings. The horizontal blue lines and numbers represent the responses for the current factor level. The desirability function approach, d or $d_i(Y_i)$, is the quality of a process that has multiple quality characteristics. The optimisation plot of both MRR and SRRR shows an ideal response value which $d_i(Y_i)$ is approach to 1 or equal to 1. Figures 6 and 7 presents the overall view of polishing parameter optimisation on MRR and SRRR respectively.

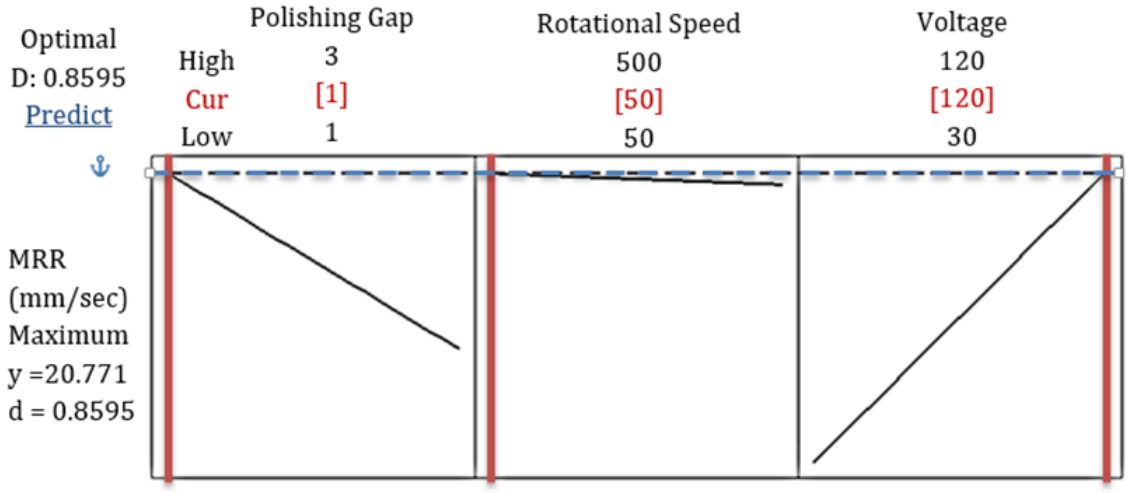

Figure 6: Optimisation plot of the polishing parameter on MRR.

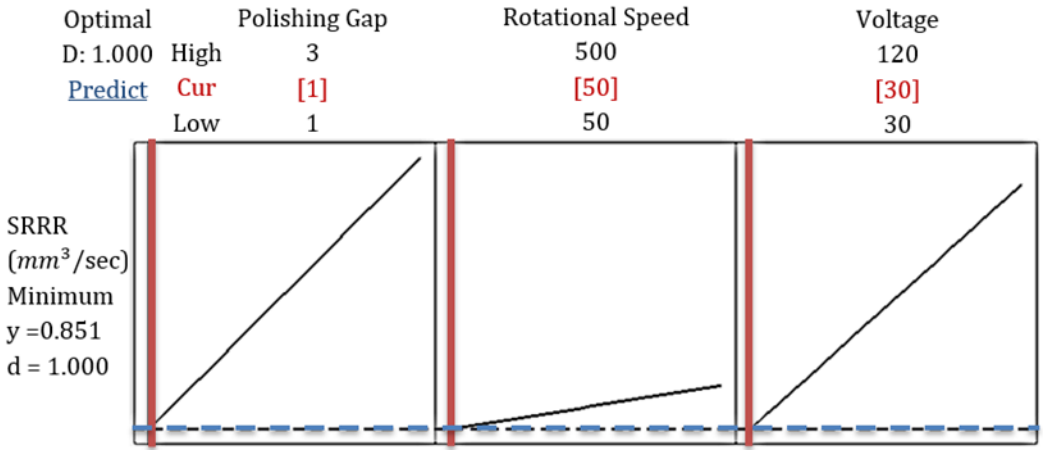

Figure 7: Optimisation plot of the polishing parameter in SRRR

The low rotational speed of 50 rpm in both MRR and SRRR obtain maximum MRR with 23.67 mm/s and 5.08 mm^3/sec respectively. A higher rotational speed, 500 rpm lead to the formation of scratches on the workpiece surface due to the abrasive alumina particle-particle alignment ruptured, thus, increased Ra. It can lead to slipping between the MR fluid and the wheel surface (Kim et al. 2008). Burr can be removed at a high geometrical precision at a specific magnetic field strength and rotational speed because at a certain level of speed the particle chain easily ruptures (Liu et al. 2016). Saraswathamma reported as the speed increases the fluid tends to flow radially and the centrifugal effects become prominent (Saraswathamma et al. 2015).

The voltage is maximum for both MRR and SRRR at 120 V and 30 V linearly increase. Maximum MRR results in 23.67 mm/sec were increasing in voltage lead to an increase of magnetic flux density, therefore, MR fluid ribbon stiffens and MRR increases (Lambropoulos et al. 2010). A stiff MR fluid enhances the alignment of the particles especially on alumina abrasive that located near to the workpiece. Meanwhile, SRRR results in a minimum, 7.37 mm^3/sec where the voltage of SRRR. Low voltage reduced the stiffness of CIP particles and lead to alumina abrasive located scattered and the force between the particles is low. Thus, low forces acted upon the workpiece and a low volume of reduction occurred.

At maximum MRR and minimum SRRR of 18.66 mm/sec and 2.74mm^3/sec, the polishing gap was at its maximum of 1 mm. A lower polishing gap increases the magnetic flux density. MR fluid flows between the gap that instantly stiffened and is in contact with the workpiece. Lowering the polishing gap can ensure that the workpiece is covered in MR fluid especially in the v-groove. A maximum voltage and maximum rotational speed may increase the shear stress, thus increasing the material removal rate during the polishing process occurs. The particles ruptured and with the maximum speed, the particles are forced to abrade the workpiece, hence, SRRR and surface roughness increase. The rotational speed is suitable and agreeable on reducing SRRR as lowering the chain structures among the particles destroyed if the rotational speed was higher.

Table 7: Table of (a) parameter and (b) solution on MRR response optimization.

(a) Parameter

Response	Goal	Lower	Upper	Target	Weight	Importance
MRR	Maximum	3.076		23.665	1	1
SRRR	Minimum		19.106	2.738	1	1

(b) Solution

	Solution	Voltage (V)	Rotational Speed (m/s)	Polishing Gap (mm)	Composite Desirability
MRR	1	120	50	1.000	1
SRRR	1	30	50	1.000	1

Table 7 shows the combination of variable settings that jointly optimize a set of responses. It evaluates the impact of voltage, rotational speed and polishing gap on SRRR and MRR. The SRRR goal was set to minimum to predict the highest desirability solutions at the upper limit to reach an efficient level. Compared to MRR which was set to the maximum goal, the lower limit is the desired result while the upper limit is the highest acceptable outcome as shown in Table 7 (a). Thus, by maximizing MRR, the efficiency of the polishing process is higher. Both MRR and SRRR were fitted with Solution 1 that achieves higher composite desirability closer to 1. The voltage is significant at 30 V, with lower voltage, SRRR value is lower while MRR increases as the voltage increase at 120 V. At the higher voltage and magnetic field, a stronger particle-particle bond between CIP and abrasive alumina developed. Therefore, higher forced acted upon to abrade the workpiece. The rotational speed for both MRR and SRRR, 50 rpm sufficiently polished the burr and scratches on the workpiece surface. On the other hand, the highest rotational speed abraded the surface more when the formation of alumina is not firmly attached by CIP due to the rupture of the particle chain. The alumina became malfunction and act as scratches on the surface.

The polishing process was efficient with a lower polishing gap as it gets near to MR fluid due to high magnetic flux density. The effective performance of the polishing process takes place on a closer polishing gap of 1 mm, which was considered between the workpiece and MR fluid surfaces. The closer the workpiece to MR fluid the higher MRR occurred in v-groove because the workpiece was covered by MR fluid as shown in Figure 8 (a) with a polishing gap of 1 mm and a lower rotational speed of 50m/s. Polishing performance best occurred with a small attachment of a flexible magnet on the edge of the workpiece as shown in Figure 8 (c), the dark black color is the flexible magnet while the grey color is MR fluid. The flexible magnet is obviously in polishing gap, rotational speed and voltage of 3 mm, 500m/s and 75V respectively due to the workpiece was polished inefficiently by MR fluid. The workpiece rotates higher and barely touches MR fluid to polish.

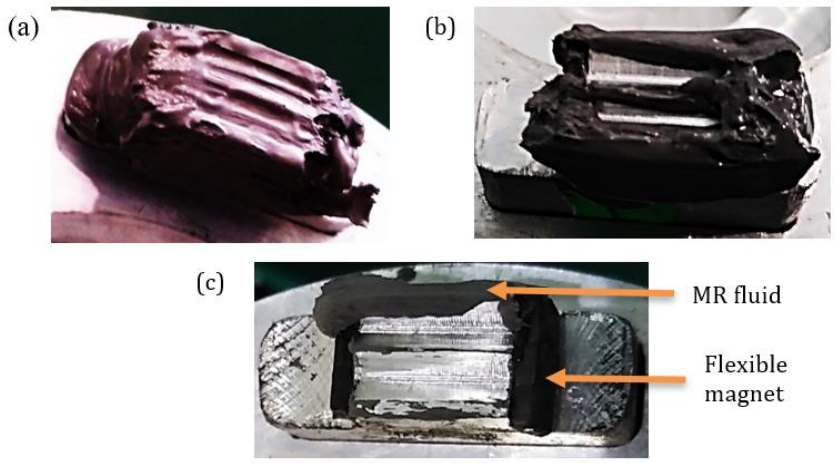

Figure 8: Workpiece covered with MR fluid with polishing gap and rotational speed of (a) 1 mm and 50m/s; (b) 2mm and 275m/s; and (c) 3mm and 500m/s respectively.

The polishing process was efficient with a lower polishing gap as it gets near to MR fluid due to high magnetic flux density. The effective performance of the polishing process takes place on a closer polishing gap of 1 mm, which was considered between the workpiece and MR fluid surfaces. The closer the workpiece to MR fluid the higher MRR occurred in v-groove because the workpiece was covered by MR fluid as shown in Figure 8 (a) with a polishing gap of 1 mm and a lower rotational speed of 50m/s. Polishing performance best occurred with a small attachment of permanent magnet on the edge of the workpiece as shown in Figure 8 (c), the dark black color is the flexible magnet while the grey color is MR fluid. The flexible magnet is obviously in polishing gap, rotational speed and voltage of 3 mm, 500m/s and 75V respectively due to the workpiece was polished inefficiently by MR fluid. The workpiece rotates higher and barely touches MR fluid to polish.

Figures 9 and 10 show is inter-related with ANOVA and the regression analysis table is shown in Table 5. Table 5 shows an interaction that occurs between the three parameters and the fitted regression interaction is plotted for MRR and SRRR in Figure 9 and Figure 10 respectively. The only interaction occurs in MRR is the polishing gap and rotational speed with p-value, 0.036 lower than $\alpha = 0.05$ as shown in the regression interaction in Figure 9. The mean value of MRR on regression analysis has a great strength between the relationship of the polishing gap and rotational speed as both of these parameters plays an important part in the MRR process. This shows that the rotational speed depends on the polishing gap; where the polishing gap is lower, the rotational speed should be lower to increase MRR value which also mentioned in Figure 6. MRR mean value linearly decreases as the polishing gap increase in rotational speed, 50 rpm at polishing gap 1mm. Meanwhile, in 500 rpm, MRR value is slightly decreased as the polishing gap increase which shows that MRR value is unbearably increased nor decrease due to particle alignment ruptured.

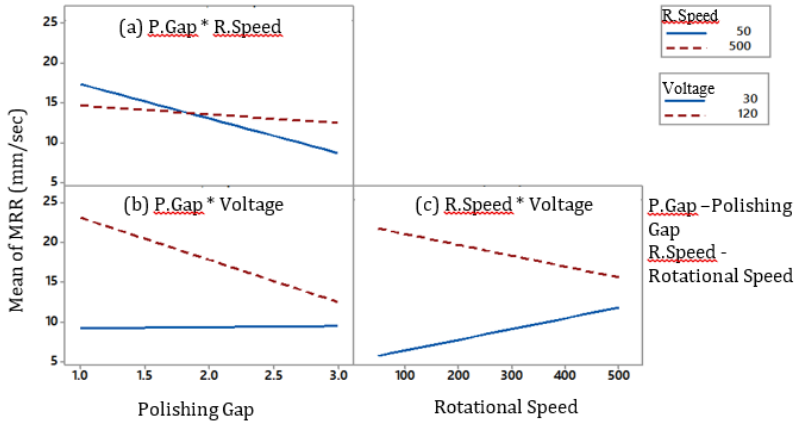

Figure 9: Interaction plot for mean of MRR between (a) polishing gap with rotational speed; (b) polishing gap with voltage; and (c) rotational speed with voltage.

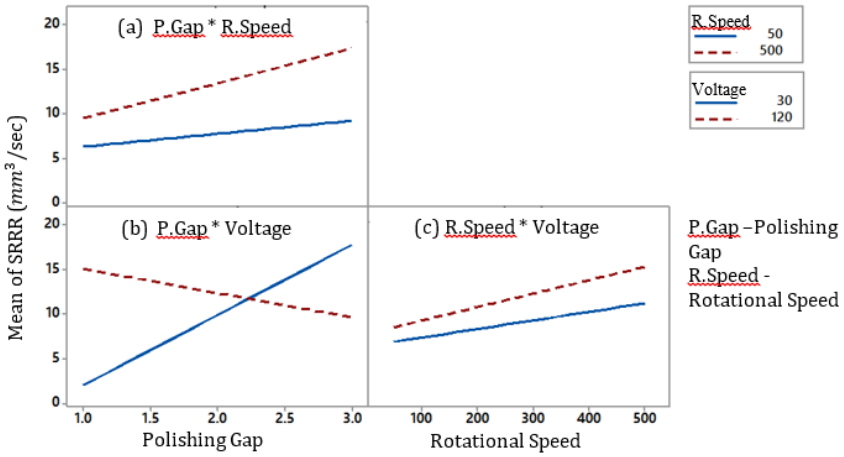

Figure 10: Interaction plot for SRRR of MR polishing between (a) polishing gap with rotational speed; (b) polishing gap with voltage; and (c) rotational speed with voltage.

The only interaction occurs in SRRR is the polishing gap and voltage with p-value, 0.002 lower than α= 0.05 as shown in the regression interaction in Figure 10. The mean value of SRRR on regression analysis has a great strength between the relationship of polishing gap and voltage as both of these parameters plays an important part in the SRRR process. This shows that the voltage depends on the polishing gap; whereas the polishing gap is lower, the voltage is lower to obtain higher SRRR value which also mentioned in Figure 7. SRRR mean value is linearly decreased as the polishing gap increase in voltage of 30 V while in 120 V, SRRR value decrease as the polishing gap increase. At 120 V with polishing gap 1mm the mean value of SRRR increases where the volume of removed of the workpiece is greater than in 30 V. This can alter the dimension of the workpiece after polishing.

3.2 Analysis of Surface Roughness

Regression analysis is performed to find out the relationship between factors and the arithmetic average of surface roughness (Ra). Using MINITAB 18 software, a statistical model based on a natural logarithm function was developed for surface roughness. The regression equation is:

$$ln(Ra) = -1.686 + 0.902\,X_1 + 0.002\,X_2 + 0.041\,X_3 - 0.112\,X_1{}^2 - 1.0\,E-06\,X_2{}^2 - 1.68E-04\,X_3{}^2 - 0.008\,X_1X_3 - 3.7E-05\,X_2X_3 + 4.85E-04\,X_1X_3 \quad (3)$$

In Figure 11, the normal probability plot is presented where the regression model completely matches the observed values. The data are consistent with samples, the points lie closer to the straight line indicates that the normal distribution is a good model for this set of data.

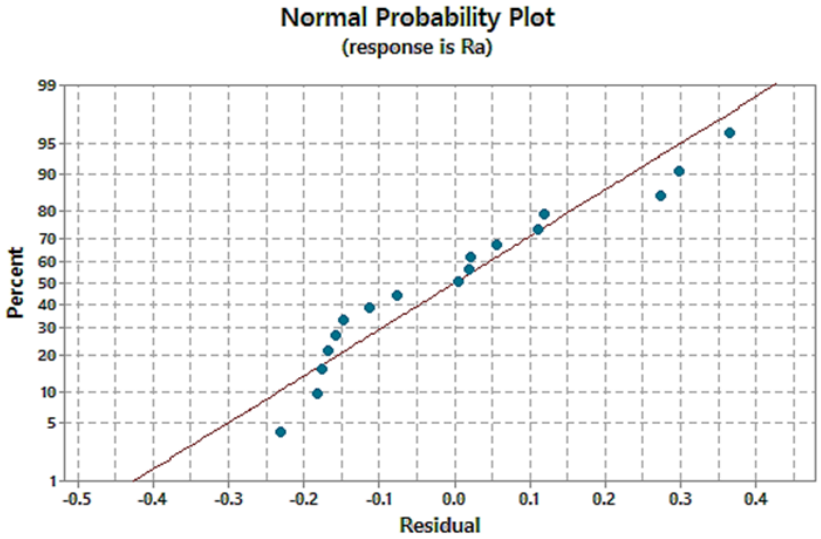

Figure 11: Normal probability plot for arithmetic average of surface roughness.

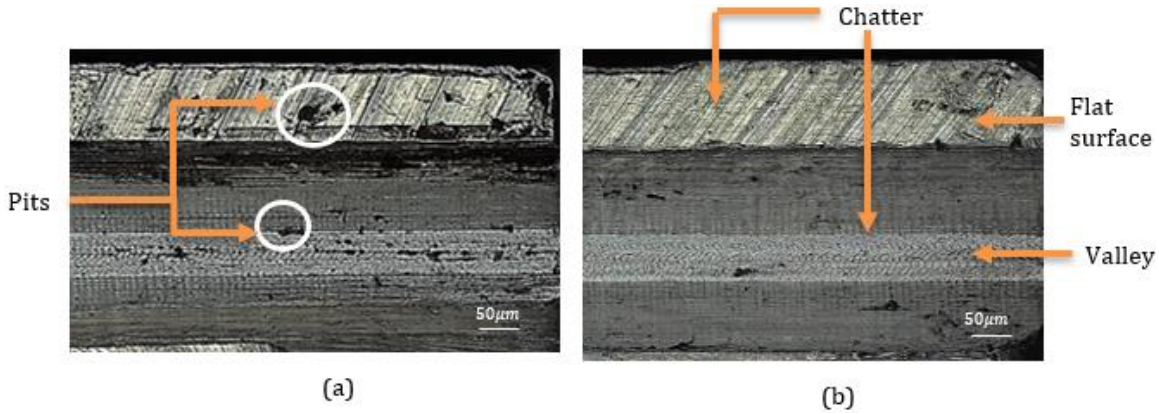

Figure 12: Profile surface on flat surface and valley (a) before polishing and (b) after polishing.

Figure 12(a) depicts the profile surface of both flat surface and valley before polishing which has numerous pits, with surface roughness, Ra=10.56μm, and Ra=4.79μm respectively. Pitting corrosion confined to a small area that takes the form of cavities as one of the most damaging forms of corrosion. The resulting pits can become wide, narrow and deep which can rapidly perforate the wall thickness of metal. Pitting corrosion is caused by the environment, lubrication liquid, and water droplet. Sufficient aeration which supplies oxygen to the reaction site enhanced the formation of oxide at the pitting site. The optimisation of the process can be achieved through response surfaces (Karkalos et al. 2016). The goal is to minimise the surface roughness as shown in 3.7 (b), where all input parameters are confined within the maximum values used in the analysis to avoid interpolation. The numerous pits were removed extensively by MR polishing. On the other hand, the waviness of the surface profile shown in Figure 12(b) is due to eccentric clamping or the form of defect of a cutter and vibration of the tool machine. Nevertheless, the result obtained has a lower surface roughness on flat surface and valley of Ra=1.15μm and Ra= 1.38μm respectively. The valley is slightly higher compared to the flat surface due to the continuous chatter of resonance that occurred during the cutting process.

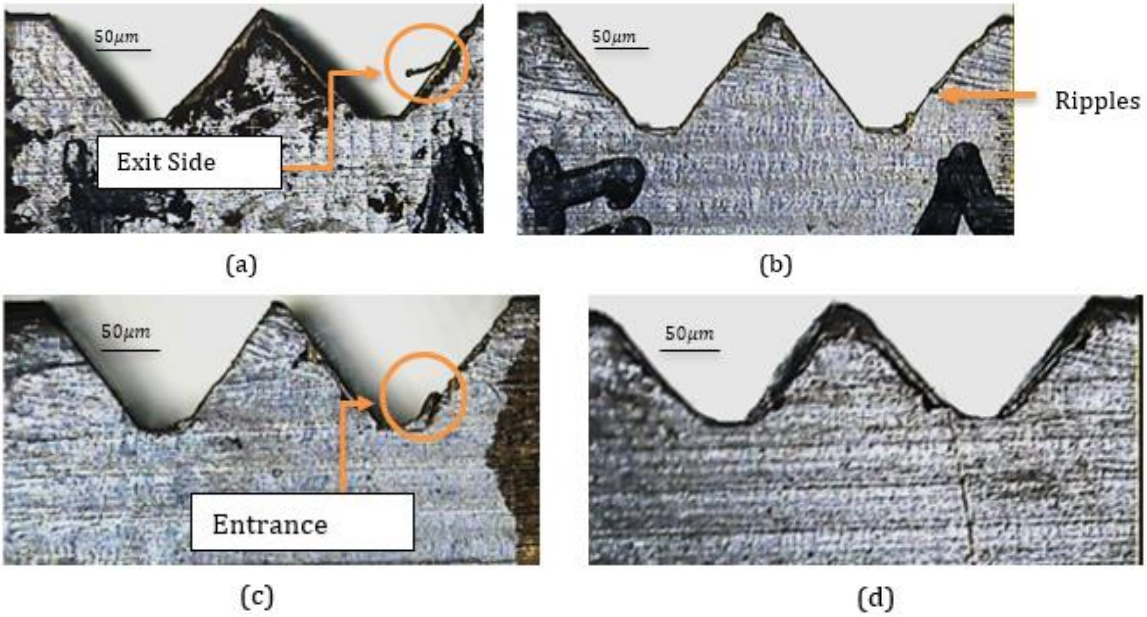

Figure 13: Surface image of v-groove (a), (c) before and, (b), (d) after polishing.

Tool wear increases surface roughness as it worsens the quality of the finished surface and formed exit side burr as shown in Figure 13. This exit side burr was always formed by milling aluminium regardless of the cutting depth and feed (Lee et al., 2012). The exit burr as shown in Figure 13(a) is at the beginning of polishing which occurred at the exit side burr with a surface roughness of Ra= 4.35μm. Lee reported that the exit burr is easier to be removed than the top burr as it attached slightly to the workpiece (Lee et al., 2012). The result obtained after polishing is as shown in Figure 13(b) where the exit side burr was effectively removed by MR fluid and the surface roughness was reduced to Ra= 0.68μm. However, there is a small part of surface irregularities also known as ripples due to the process of MR particles (alumina abrasive particle).

Figure 13(c) shows an entrance burr on the workpiece before polishing occurred due to a higher feed rate. The burr slightly increases the surface roughness to Ra= 8.01μm. Entrance burr formed curl-type burr due to tool chipping. This tool chipping was severe until it was being pushed and bent over the edge. Figure 13 shows the lowest surface roughness value of Ra= 0.41μm.

4.0 CONCLUSION

The paper aims to fabricate a new method of MR fluid-assistive polishing for metal microfeatures. The work adopts a 1 d.o.f 2 axis of magnetorheological polishing rig machine. The performance of the magnetorheological polishing rig process was successfully evaluated on aluminium AISI 6061 workpiece surface for flat surface, valley and v-groove. The derivation of the mathematical models for material removal rate and surface roughness reduction ratio were taking into account the voltage, rotational speed, and the polishing gap. The result shows that the voltage is dominated by the polishing rig as the magnetic field supplied the main source towards the polishing rig. To determine the optimal polishing conditions using alumina abrasives in MR fluid; the material removal, surface roughness reduction ratio and surface roughness of polishing spots were measured by altering the voltage, rotational speed, and polishing gap. The surface roughness that consists of burr formation and surface irregularities has reduced. The minimum surface roughness was 1.15μm, 1.38μm, and 0.41μm on a flat surface, valley, and v-groove respectively. Increasing voltage increases the material removal rate which leads to a low surface roughness reduction ratio. The specific rotational speed of 227.27rpm generates a low surface roughness reduction ratio and a better performance since the polishing did not remove a higher volume which disrupts the dimension of the workpiece. However, it was observed that the material removal rate decreases after a certain level of speed, especially at a lower rotational speed.

ACKNOWLEDGEMENT

The authors would like to acknowledge Universiti Malaysia Pahang and the Ministry of Education Malaysia for funding this research under Fundamental Research Grant Scheme (FRGS/1/2016/TK03/UMP/02/12- RDU160132) and thanks too Keyence 3D Laser Scanning Confocal Microscope.

REFERENCES

Abukhshim, N. A., Mativenga, P. T., & Sheikh, M. A. (2006). Heat generation and temperature prediction in metal cutting: A review and implications for high speed machining. International Journal of Machine Tools and Manufacture, 46(7-8), 782-800.

Alam, Z. et al., 2018. Nanofinishing of 3D surfaces by automated five-axis CNC ball end magnetorheological finishing machine using customized controller. International Journal of Advanced Manufacturing Technology, pp.1–12.

Cheng, H.B., Feng, Y.P., et al., 2009. Material removal and micro-roughness in fluid-assisted smoothing of reaction-bonded silicon carbide surfaces. Journal of Materials Processing Technology, 209(9), pp.4563–4567.

Cheng, H.B., Yam, Y. & Wang, Y.T., 2009. Experimentation on MR fluid using a 2-axis wheel tool. Journal of Materials Processing Technology, 209(12–13), pp.5254–5261.

Gopal, D., Ganapathy, R.B.B.R. & Palani, S.R., 2017. STUDY THE MACHINING PROCESS OF MAGNETORHEOLOGICAL FLUID. , (June).

Jang, K. I., Kim, D. Y., Maeng, S., Lee, W., Han, J., Seok, J., ... & Min, B. K. (2012). Deburring microparts using a magnetorheological fluid. International Journal of Machine Tools and Manufacture, 53(1), 170-175.

Jha, S. (2015). Design of Parallel Plate Magnetorheometer for evaluating properties of Magnetorheological polishing fluid. Materials Today: Proceedings, 2(4-5), 3251-3259.

Kang Hyun Song, Bong Jun Park & Hyoung Jin Choi, 2009. Effect of Magnetic Nanoparticle Additive on Characteristics of Magnetorheological Fluid. IEEE Transactions on Magnetics, 45(10), pp.4045–4048.

Kim, D.-W. et al., 2008. Experimental Study on the Effects of Alumina Abrasive Particle Behavior in MR Polishing for MEMS Applications. Sensors, 8(1), pp.222–235.

Kolari, K., 2008. Deep plasma etching of glass with a silicon shadow mask. , 141, pp.677–684.

Kumar, K. S., Senthilkumaar, J. S., & Srinivasan, A. (2013). Reducing surface roughness by optimising the turning parameters. South African Journal of Industrial Engineering, 24(2), 78-87.

Lambropoulos, J. C., Miao, C., & Jacobs, S. D. (2010). Magnetic field effects on shear and normal stresses in magnetorheological finishing. Optics express, 18(19), 19713-19723.

Liu, H. et al., 2016. Configuration design and accuracy analysis of a novel magnetorheological finishing machine tool for concave surfaces with small radius of curvature †. , 30(7), pp.3301–3311.

Luo, X. et al., 2005. Design of ultraprecision machine tools with applications to manufacture of miniature and micro components. Journal of Materials Processing Technology, 167(2–3), pp.515–528.

Miao, C., Jacobs, S.D. & Program, M.S., 2009. Frictional Forces in Material Removal for Glasses and Ceramics Using Magnetorheological Finishing Curriculum Vitae.

Park, J. H., Lee, N. E., Lee, J., Park, J. S., & Park, H. D. (2005). Deep dry etching of borosilicate glass using SF6 and SF6/Ar inductively coupled plasmas. Microelectronic engineering, 82(2), 119-128.

Rahim, M.S.A. et al., 2016. Magnetic field simulation of a thermal conductivity measurement instrument for magnetorheological fluid. MATEC Web of Conferences, 90, p.1061.

Saptaji, K., & Subbiah, S. (2017). Burr reduction of micro-milled microfluidic channels mould using a tapered tool. Procedia engineering, 184, 137-144.

Sidpara, A., & Jain, V. K. (2012). Nano–level finishing of single crystal silicon blank using magnetorheological finishing process. Tribology International, 47, 159-166.

Singh, A. K., Jha, S., & Pandey, P. M. (2012). Nanofinishing of a typical 3D ferromagnetic workpiece using ball end magnetorheological finishing process. International Journal of Machine Tools and Manufacture, 63, 21-31.

Skalski, P., & Kalita, K. (2017). Role of magnetorheological fluids and elastomers in today's world. acta mechanica et automatica, 11(4), 267-274.

Song, W.L. et al., 2013. Finishing performance of magneto-rheological fluid under magnetic field. Mechanics of Advanced Materials and Structures, 20(7), pp.529–535.

Tingzhang, W., Mingjun, C., Henan, L., & Jiang, X. (2015). Development of a Magnetorheological Finishing Machine for Small-Bore Part of Irregular Shape and Experimental Study. American Journal of Engineering and Applied Sciences, 8(3), 399.

Tricard, M. et al., 2003. SOI wafer polishing with magnetorheological finishing (MRF). SOI Conference, 2003. IEEE International, (585), pp.127–129.

Wang, Y. et al., 2015. Identification and compensation for offset errors on the rotary axes of a multi-axis Magnetorheological Finishing machine tool. International Journal of Advanced Manufacturing Technology, 78(9–12), pp.1743–1749.

Wang, Y., Yin, S. & Huang, H., 2016. Polishing characteristics and mechanism in magnetorheological planarization using a permanent magnetic yoke with translational movement. Precision Engineering, 43, pp.93–104. Available at: http://dx.doi.org/10.1016/j.precisioneng.2015.06.014.

Wiltsie, N., Lanzetta, M. & Iagnemma, K., 2012. A controllably adhesive climbing robot using magnetorheological fluid. 2012 IEEE Conference on Technologies for Practical Robot Applications, TePRA 2012, pp.91–96.